In Memory of Professor Hsun HU

Textures of Materials

Proceedings of the Eleventh International Conference on Textures of Materials

Volume 1

ICOTOM-11

September 16-20, 1996

Xi'an, China

Edited by

Zhide LIANG

Liang ZUO

Youyi CHU

International Academic Publishers

图书在版编目(CIP)数据

材料织构：第十一届国际材料织构会议论文集：英文/梁志德等编. －北京：万国学术出版社，1996.9
ISBN 7-80003-376-7

Ⅰ.材… Ⅱ.梁… Ⅲ.金属－材料－织构－国际会议－文集－英文 Ⅳ.TG14-53

中国版本图书馆 CIP 数据核字（96）第 11602 号

Published and Distributed by
International Academic Publishers
137 Chaonei Dajie, Beijing 100010
The People's Republic of China

The book has been photographically reproduced from the bestavailable copy. The papers were not refereed but were reviewed for their technical contents. Editing was restricted to matters of format, general organization and retyping.

The editors assume no responsibility for the accuracy, completeness or usefulness of the information disclosed in this volume. Unauthorized use might infringe on privately owned patents of publication right. Please contact the individual authors for permission to reprint or otherwise use information from their papers.

First edition 1996

Liang Zhide, Zuo Liang and Chu Youyi
Textures of Materials Vol. 1
— Proceedings of the Eleventh International Conference on Textures of Materials

ISBN 7-80003-376-7/TG.26

Printed by the Printing House of China Building Industry Press

ROLLING AND ANNEALING TEXTURES OF A FERRITIC STAINLESS STEEL WITH 11 MASS%CR CONTENT

D. Raabe

Institut für Metallkunde und Metallphysik,
RWTH Aachen, Kopernikusstr.14, 52056 Aachen, Germany

ABSTRACT

The hot rolling, cold rolling and annealing texture of a ferritic stainless steel with 11% Cr content was studied. The hot and cold rolled sheet revealed a through thickness texture gradient. In the center layer of the hot band a cold rolling texture (α-fiber) was observed which was attributed to ideal plane strain deformation and strong recovery. Close to the surface a strong Goss orientation was detected which was attributed to shear deformation. During cold rolling the inherited texture sharpened in the center layer and decreased in the subsurface layer, i.e. Goss oriented grains rotated either towards the α-fiber or towards {111}<112>. The evolution of the cold rolling texture was simulated by use of a Taylor type model considering both the starting texture and the grain morphology. Final annealing led to a γ-fiber and to a weak {001}<110> texture component which was retained by recovery. Due to the inhomogeneous hot and cold rolling texture the annealing texture was inhomogeneous through the sheet thickness as well.

Keywords: Ferritic Stainless Steel, 11% Cr, Texture Inhomogeneity, Simulation

INTRODUCTION

The texture evolution of ferritic stainless steels with 16%-17% (%=mass%) Cr content has been the subject of numerous studies [1-6]. However, except for some recent investigations on rolling texture evolution [7] the examination of steels containing 10%-11% Cr has not yet been tackled accordingly in the literature. These low alloyed ferritic stainless steels represent a competitive class of materials for many technical applications which are presently reserved for Fe-17%Cr. This investigation is concerned with the evolution of the rolling and annealing texture of Fe-11%Cr steels with special regard to texture inhomogeneity. It is well known from Fe-17% Cr steels [1-6], that the phenomenon of texture inhomogeneity generated during hot rolling has considerable influence on recrystallization subsequent to cold rolling, i.e. it can influence the properties of the final material.

EXPERIMENTAL

A continuously cast and hot rolled ferritic stainless steels containing 10.5% Cr (%=mass%) was investigated (Table 1). The steel was unidirectionally hot rolled, passing 7 four high stands, to a final thickness of 3 mm. The first pass was carried out within the temperature range, 1400K to 1460K and the last one within the range, 1200K to 1300K. After hot rolling the steel was annealed at 1300 K. Cold

rolling was carried out to ε=40%, 55%, 70%, 80% and 90% (ε=Δd/d). The samples were rotated 180° about the transverse direction after each pass. Since homogeneous deformation is primarily determined by the ratio of contact length, l_d, to sheet thickness, d, a ratio of $1 < (l_d/d) < 3$ was obtained during cold rolling. Recrystallization was carried out at 1170 K in a salt bath furnace for 5 minutes.

Table 1 Chemical composition of the stainless steel (balance Fe), mass%.

Cr	C	N	Ti	Nb
10.5	0.01	0.02	0.11	0.32

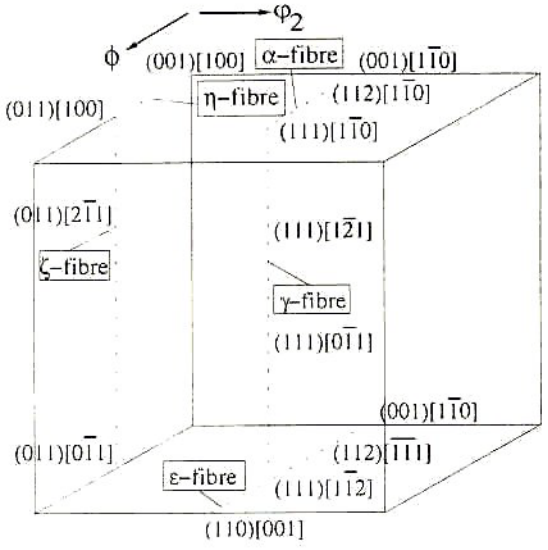

Fig. 1 Euler space with some relevant texture fibers.

The textures were examined by measuring the four incomplete pole figures {110}, {200}, {112} and {103} in the range of the pole distance angle α from 5° to 85° using $Mo_{K\alpha}$ radiation in the back reflection mode [8]. The orientation distribution function (ODF) was derived by using the iterative series expansion method in the version of Dahms et al. [9-11]. This method makes use of two additional assumptions which yield considerable improvements of pole figure inversion as compared to the conventional method. The first ingredient added, referred to as the non-negativity condition, implies that negative pole densities are physically meaningless [9,10,12]. The second condition included, is the so called 'phone concept' [13], where the term 'phone' describes an isotropic background component. This condition increases the non-negativity constraint in such a way that the minimum pole densities of the unmeasured recalculated pole figures are not only set equal to zero but to the pole density of the phone component. In order to reduce truncation errors a series expansion degree of $l_{max} = 34$ was used throughout this study.

BCC (body centered cubic) metals and alloys tend to develop strong fiber textures [e.g. 4]. It is hence convenient to characterize the ODF in terms of texture fibers, which can be presented using iso-intensity diagrams (φ_1-sections) or so called fiber diagrams [e.g. 4], Fig. 1. The most relevant texture fibers, employed in the current study are the α-fiber, which contains all {hkl}<110> orientations, the γ-fiber, which comprises all {111}<uvw> orientations, the η-fiber containing all {hkl}<001> components and the ε-fiber which includes all orientations with a crystal <110> axis arranged parallel to the transverse direction. Finally, the β-skeleton line is used for depicting texture maxima in the immediate vicinity of the γ-fiber. The latter fiber is especially relevant for discussing recrystallization textures of steels [5].

As is well known from Fe-17%Cr [1-6] the texture and microstructure of ferritic stainless steels is very inhomogeneous through the sheet thickness. As was shown in a preceding investigation [7] this seems to apply also for Fe-11%Cr. All samples were thus measured in four different through-thickness layers. The layer under investigation is described by the so called parameter s, which indicates the distance between layer and sample center devided by the half thickness (s=0 center, s=1 surface). In order to remove a layer of 20·μm the samples were etched in a solution of 50 ml H_2O_2 and 10 ml HF prior to the texture measurement.

RESULTS AND DISCUSSION

1. Hot Rolling

Hot rolling was industrially carried out using seven uni-directional rolling passes. Owing to its Cr and C content, the alloy under investigation undergoes about 20vol.% phase transformation during the first hot rolling steps [14,15]. During the last hot rolling step the transformed volume fraction was assessed not to exceed 10% [14,15].

Fig. 2 (center layer) and Fig. 3 (sub-surface layer) show the texture of the hot and cold rolled sample. In the center layer of the hot band (ε=0%) a strong α-fiber, accompanied by a weak γ-fiber is developed. Close to the surface layer a very strong {011}<100> component, which is referred to as Goss component, and a very weak α-fiber is formed. This type of hot band texture is well known from Fe-17%Cr [1-5].

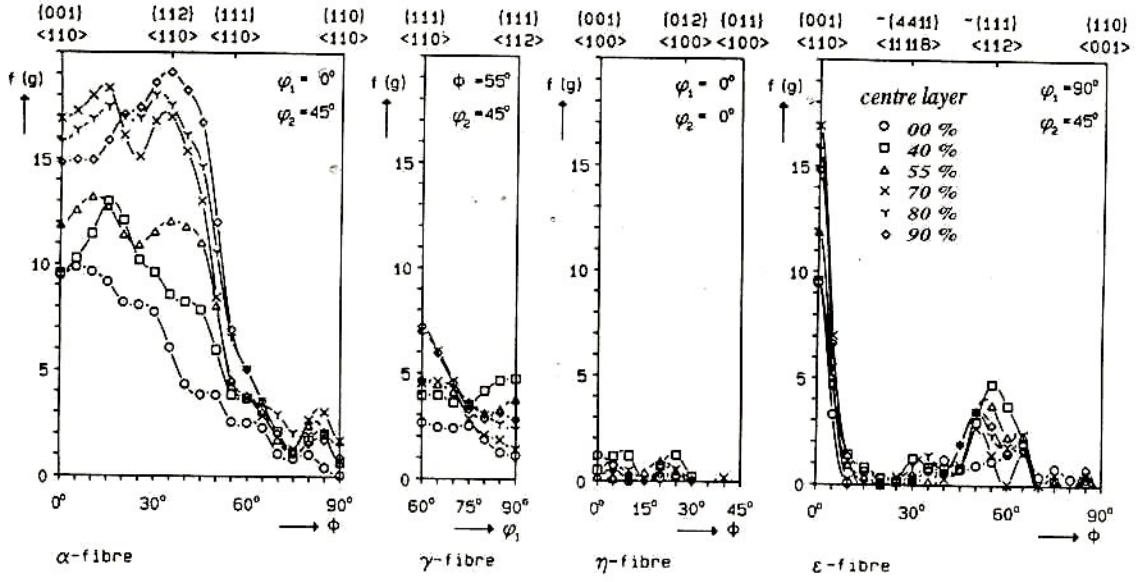

Fig. 2 Evolution of cold rolling texture in fiber presentation, center layer (s=0), ε=0 : hot band texture.

In a previous investigation it was shown that the microstructure reveals considerable differences between the center and the sub-surface layer [7]. Whereas in the center layer the volume fraction recrystallized amounted to less than 5%, in the sub-surface layer 52% of the volume had undergone primary recrystallization. Two conclusions can be drawn from the microstructure and texture. First, the center layer texture of the hot band obviously represents a typical cold rolling type of texture, since neither massive phase transformation, nor recrystallization have taken place. Second, close to the surface layer, the influence of massive recrystallization has to be considered [7]. However, in the corresponding texture (Fig. 3) no typical texture components, known from static, primary recrystallization are apparent.

The Goss orientation is an exception, since it can be attributed to both deformation and recrystallization. From the literature it is know [1-5,16,17] that the formation of Goss close to the surface of ferritic steels is attributed to heavy shear deformation. However, the Goss orientation is also known from Fe-Si, Fe-17%Cr or low carbon steels with large grains to nucleate in shear or transition bands during recrystallization [e.g. 4]. If these inhomogeneities are situated in {111}<112> oriented crystals and reveal a 35° inclination about the transverse direction (which transforms {111}<112> into Goss), a growth into the surrounding matrix is conceivable during annealing. However, Goss oriented grains the formation of which was attributed to such a mechanism have in Fe-Cr alloys been reported to not exceed a few volume fraction [1]. Moreover, in the present case no strong {111}<112> texture component is observed. The

mechanism mentioned is thus assumed to be relevant for primary recrystallization after cold rolling rather than for hot rolling. However, in order to attribute the Goss component observed to shear deformation, reliable data about the strain distribution in the hot band are required.

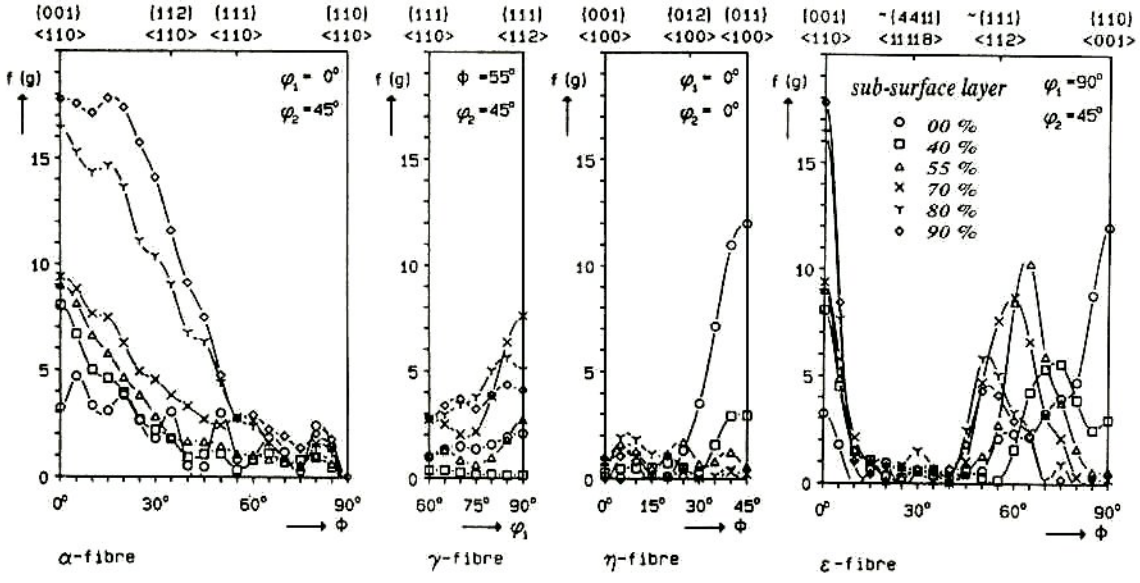

Fig. 3 Evolution of cold rolling texture in fiber presentation, sub-surface layer (s=0.8), ε=0 : hot band texture.

Such data were given in various studies [e.g. 18]. Among various definitions employed to compute the through-thickness profiles of the equivalent strain, those which accounted either for the strain rates or for the accumulation of shear strains irrespective of their sign, yielded the highest shear strains at s=0.8 [18]. This position corresponds indeed to the maximum of the Goss orientation. From both, texture and microstructure as well as simulations it is hence suggested that the Goss component observed close to the surface after hot rolling is attributed to heavy shear deformation. The strong cold rolling texture observed in the center layer is interpreted as rolling texture with a negligible influence of recrystallization.

2. Cold Rolling

Owing to its inhomogeneous hot band texture the steel under investigation reveals a very similar texture evolution during cold rolling as stainless steels with 17% Cr [1-6]. After ε=40% in the center layer a strong α-fiber texture ranging from {001}<110> to {111}<110> accompanied by a weak {111}<112> component has developed (Fig. 2). This texture is inherited from the hot band and has been sharpened during subsequent cold rolling. In the sub-surface layer a considerable texture change place (Fig. 3). Since grains with an initial Goss orientation are no longer stable under plane strain conditions imposed during cold rolling they rotate either towards {001}<110> (α-fiber) or {111}<112> (γ-fiber). From Fe-17%Cr it was reported that some Goss oriented grains generated during hot rolling even undergo grain fragmentation due to locally opposite rotations [1]. Figs. 2 and 3 substantiate that even after 40% cold reduction a strong texture gradient is still apparent.

After ε=55% in the center layer the α-fiber is increased. In the sub-surface layer the Goss component is completely degraded and a weak α-fiber texture, mainly consisting of a pronounced {001}<110> orientation is developed. Both, the {001}<110> as well the {111}<112> component, the orientation density of which is much higher than in the center layer, are generated by formerly Goss oriented crystals. After ε=70% the center layer texture is again increased. In the sub-surface layer the initially isolated {001}<110> orientation observed on the α-fiber appears considerably spread out towards {112}<110>

and {111}<110>. With ongoing deformation the texture in both layers becomes more and more similar to each other. However, even up to ε=90% cold reduction the maximum orientation density in the center layer remains higher than that observed in the sub-surface texture.

3. Simulation of the Cold Rolling Textures

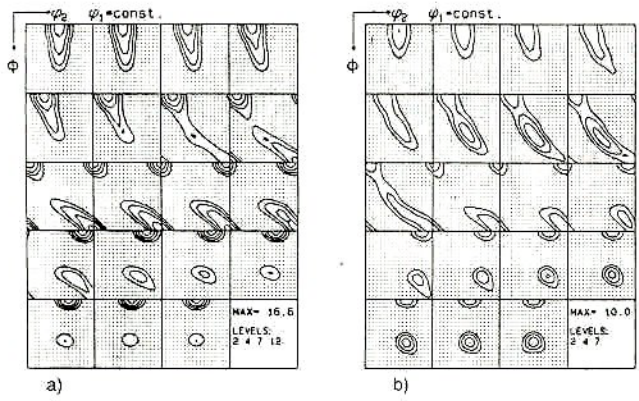

Fig. 4 Taylor simulation, ε=55%, a) s=0, b) s=0.8.

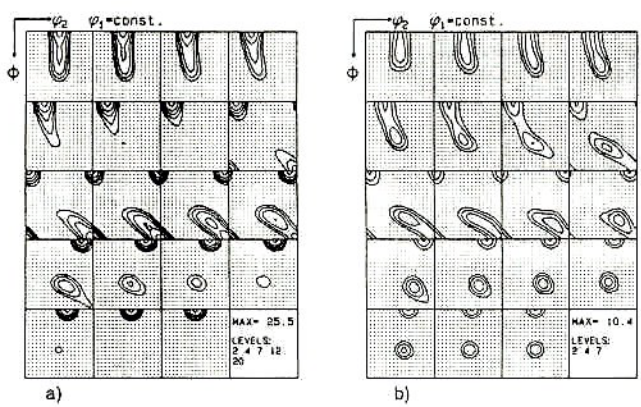

Fig. 5 Taylor simulation, ε=80%, a) s=0, b) s=0.8.

The observed textures can be explained in terms of Relaxed Constraints Taylor Theory [19]. The cold rolling textures of both layers (s=0, s=0.8) were simulated by using a Taylor model which accounts for the grain morphology. Due to the flat and elongated grain shapes observed in the center layer [7] the simulations of the textures at s=0 are carried out by relaxation of the ε_{13} and ε_{23} shear constraints (pancake-model) (1=RD, 3=ND). In comparison, the texture simulation at s=0.8 are for low strains carried out by releasing the ε_{13} strain constraint (lath model). For strains exceeding 70%, the ε_{23} component is additionally relaxed. Although this scheme is to a certain extent arbitrary it is assumed that the flat grains observed in the sheet center allow pancake type deformation. In comparison, close to the surface this model does presumably exclusively hold for large strains since it was shown that in the initial sheet 52% of the grain volume is recrystallized, i.e. equiaxed rather than flat. However, only the latter type of grain shape justifies application of the pancake model. In the present study {110}, {112} and {123} slip planes each containing a ½ <111> Burgers vector have been considered with identical critical resolved shear stresses. For the simulation of cold rolling the hot rolling textures were used as starting point. For this purpose the hot band ODFs were decomposed into 830 (s=0) and 715 (s=0.8) single orientations. Cold rolling was simulated by imposing ideal plane strain conditions. For computing the resulting ODFs each orientation was superimposed by a Gauss function, applying a scatter width of 8° in accord with local orientation gradients observed in Fe grains [20]. Fig. 4a shows that for ε=55% the relevant features of the experimental texture are covered. Both, the α-fiber with a maximum close to {001}<110> and the weak {111}<112> component are well predicted. However, the simulated texture is somewhat stronger than the experimental one. The texture simulated for s=0.8 (Fig. 4b) also reveals good correspondence to the experimental ODF. The evolution of the α-fiber as well as the orientation density at {111}<112> are nearly identical to those determined experimentally. After ε=80% the simulated center layer texture (Fig. 5a) yields a correct description of the experimental ODF. However, in the simulated texture the {001}<110> orientation is more pronounced than in the experimental one. The simulated ODF in the sub-surface layer (Fig. 5b) reveals a lower maximum than the experimental one. This deviation is attributed to the transition from the lath to the pancake model.

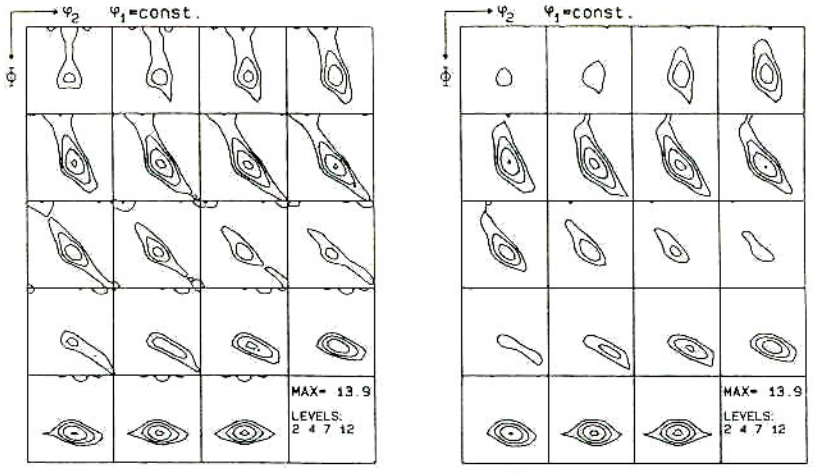

a) b)

Fig. 6 Recrystallization texture, ε=80% cold rolled , 1170 K, salt bath furnace, annealing time : 5 minutes a) s=0, b) s=0.8.

4. Recrystallization

Fig. 6 shows the annealing texture of the 80% cold rolled sample in two through-thickness layers. The texture is generally characterized by the degradation of the α-fiber components and the increase of the γ-fiber. In the center layer the α-fiber is only partially removed which is attributed to recovery.

REFERENCES

1. D. Raabe and K. Lücke: Mat. Sc. and Techn. 9 (1993), 302.
2. M. Hölscher, D. Raabe and K. Lücke: Acta Metall. 42 (1994), 879.
3. D. Raabe: Mat. Sc. and Techn. 11 (1995), 461.
4. D. Raabe and K. Lücke: Proc. 10th Int. Conf. on Tex. of Mat. ICOTOM 10, Materials Science Forum, 157-162 (1994), 1469.
5. D. Raabe and K. Lücke: Steel Research 63 (1992), 457.
6. D. Raabe, M. Hölscher, M. Dubke, H. Pfeifer, H. Hanke and K. Lücke: Steel Research 64 (1993), 359.
7. D. Raabe : Mat. Sc. and Techn. 11 (1995) 985.
8. L. G. Schulz: Journ. Appl. Phy. 20 (1949), 1030.
9. M. Dahms, H.J. Bunge: J. Appl. Cryst. 22 (1989), 439.
10. M. Dahms: Text. and Microstr. 19 (1992), 169.
11. D. Raabe: Text. and Microstr. 23 (1995) 115.
12. H. R. Wenk, H. J. Bunge, J. Kallend, K. Lücke, S. Matthies, J. Pospiech, P. van Houtte: Proc. 8th Int. Conf. on Tex. of Mat. ICOTOM 8, ed. J. Kallend, G. Gottstein, The Metall. Soc. (1988), 17.
13. S. Matthies: Proc. 7th Int. Conf. on Tex. of Mat. ICOTOM 7, ed. C. M. Brakman, P. Jongenburger and E. J. Mittenseijer, Netherl. Soc. for Mater. Sci., Noordwijkerhout (1984), 737.
14. E. Houdremont, Handb. Sonderstahlkunde, 3. Aufl., Springer Verlag 1 (1956), 623.
15. K. Bungardt, E. Kunze and E. Horn: Arch. Eisenhüttenw. 29 (1958), 193.
16. R.O. Williams: Trans. AIME 224 (1962), 129.
17. W. Österle and H. Wever: Z. Metallkunde 72 (1981), 230.
18. A. J. McLaren and C. M. Sellars: Mat. Sc. and Techn. 8 (1992), 1090.
19. H. Honneff and H. Mecking: Proc. 5th Int. Conf. on Tex. of Mat. ICOTOM 5, ed. G. Gottstein and K. Lücke, Springer Verlag (1978), 265.
20. D. Raabe: phys. stat. sol. (b) 181 (1994), 291.